Publ. Astron. Soc. Japan (2014) 00(0), 1–6
doi: 10.1093/pasj/xxx000

Giant HI Hole in the Galactic Halo inside the 3-kpc Ring and the North Polar Spur

Yoshiaki SOFUE[1]

[1]Insitute of Astronomy, The University of Tokyo, Mitaka, Tokyo 181-0015, Japan

*E-mail: sofue@ioa.s.u-tokyo.ac.jp

Received ; Accepted

Abstract

This paper reports the discovery of a giant HI hole of radius ~ 3 kpc in the Galactic halo around the Galactic Centre. The tangential edge of the hole is located at $l \sim \pm 20^\circ$ ($R = 2.9$ kpc in radius), where an HI wall vertically emanates from the 3-kpc expanding ring (at $R = 2.7$ kpc). The wall extends up to height of ~ 1.3 kpc from the galactic plane, and positionally coincides with the radio continuum North Polar Spur. The HI hole is explained as due to sweeping of the halo gas by a shock-wave from the Galactic Centre. The vertical density distribution of the unperturbed HI halo outside the ring is represented by a $\mathrm{sech}^2 Z/\zeta$ density profile with scale height $\zeta \sim 500$ pc.

Key words: Galaxy: centre – Galaxy: kinematics and dynamics – Galaxy: halo – ISM: atoms – radio lines: ISM
– radio continuum: ISM

1 Introduction

Among the number of expanding features in the Galactic disc, the most massive object is known as the 3-kpc ring recognized as an inclined ellipse in the HI- and CO-line longitude-velocity (LV) diagrams (Cohen and Davies 1976; Bania 1977; Oort 1977 for review; Dame and Thaddeus 2008; Garcia et al. 2014). The near-side arm of the 3-kpc ring is approaching, and therefore, expanding at velocity of $V_{\rm expa} \sim 53$ km s^{-1}(Cohen and Davies 1976; Oort 1977), and the far-side is receding at $V_{\rm expa} \sim 56$ km s^{-1}(Dame and Thaddeus 2008).

From the expanding nature, the structure has been interpreted as an expanding ring driven by a central explosive activity (Sanders and Prendergast 1974; Oort 1977; Sofue 1976, 1977; 1984; 1994; 2000; 2017; Sofue et al. 2016). On the other hand, as the Galaxy is evidenced to be barred, the non-circular motion has been believed to be due to an oval flow in the bar potential (Mulder and Liem 1986; Binney et al. 1991; Englmaier and Gerhard 1999; Fux 1999; Rodriguez-Fernandez and Combes 2008; Baba et al. 2010).

The explosion hypothesis has recently been revisited according to accumulating evidence for energetic phenomena in the GC such as the bipolar hypershells (BHS) in radio and X-rays including the North Polar Spur (Sofue 2016; and the literature therein) and the Fermi Bubbles in γ-rays (Su et al. 2010). It should be stressed that, if the Galaxy is barred, the explosive activity in the GC is the inevitable consequence of the bar-shocked gas accretion (Sofue 2017).

In this paper, we examine the relationship between the 3-kpc HI ring and radio spurs using the existing survey data. We model the origin of the ring by the propagtion of a BHS shock wave through the galactic halo. In the analysis, the solar distance from the Galactic Centre (GC) is assumed to be $R_0 = 8$ kpc and the rotation velocity $V_0 = 238$ km s^{-1}(Honma et al. 2015).

2 Radio and HI Maps

2.1 Radio continuum spurs

Figure 1 shows backgound filtered (BGF/unsharp-masked) maps of the 408, 1420 and 2300 MHz continuum emission around the GC produced from the all-sky radio continuum surveys by Haslam et al. (1982), Reich et al. (2001a, b) and Jonas

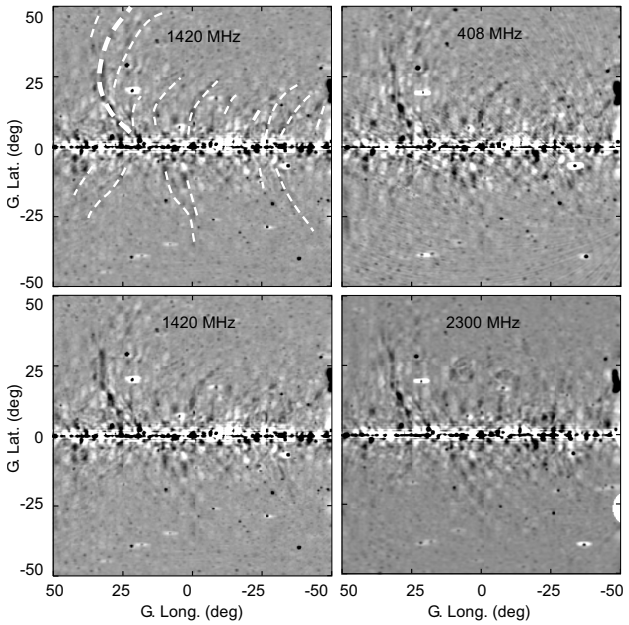

Fig. 1. Intensity excess maps at 408, 1420 and 2300 MHz continuum maps as produced from the all-sky radio surveys by Haslam et al. (1982), Reich et al. (2001a, b), and Jonas et al. (1998), respectively. Dashed lines indicate radio spurs.

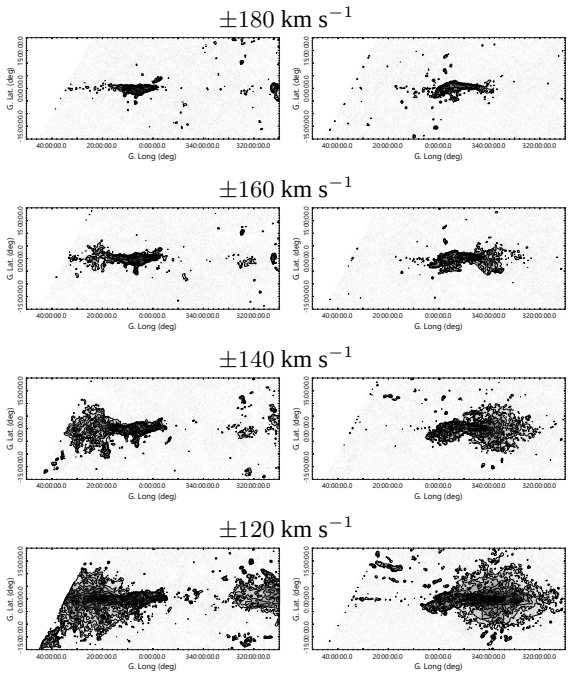

Fig. 2. HI channel maps as produced from the Parkes HI survey GASS (McClure-Griffiths et al. 2009; Kalberla et al. 2010)

et al. (1998), respectively. The BGF intensity excess is here defined as

$$\Delta T = T_{\rm B}/\bar{T}_{\rm B} - 1, \tag{1}$$

where $T_{\rm B}$ is the brightness temperature and $\bar{T}_{\rm B}$ is the smoothed intensity in an area $\delta l \times \delta b = 5^\circ \times 1^\circ$ around each data point. Marked by the dashed lines are the radio spurs NPS, NPS-E, South Polar Spur (SPS), and SPS-W (Sofue 2000).

2.2 HI map

Figure 2 shows channel maps of HI brightnes temperature T in the central $\pm 50^\circ \times \pm 20^\circ$ region at $V_{\rm lsr} = \pm 120,\ \pm 140,\ 160$ and 180 km s^{-1} as produced by using the Parkes HI survey GASS (McClure-Griffiths et al. 2009; Kalberla et al. 2010).

The major HI disc is recognized as the dense and tight ridge with full width $\sim 1^\circ$ at velocities from $V_{\rm lsr} \sim \pm 200$ to ± 160 km s^{-1}, and can be traced in the maps up to $\sim \pm 100$ km s^{-1}at peak brightness $T \sim 50 - 100$ K.

At $V_{\rm lsr} \sim \pm 130$ km s^{-1}corresponding to the tangent longitude of $l \sim 20^\circ$, a remarkable change of distribution occurs so that a vertically extended component suddenly appears as an HI flare (wall) toward high latitudes. The brightness of the flare is $T \sim 1 - 2$ K, less bright than the main disc, and the latitudinal extension is as large as $b \pm 10^\circ$, or it reaches altitutdes $Z \sim \pm 1.3$ kpc.

In figure 3 we enlarge the channel maps at ± 130 km s^{-1}, and overlay the radio continuum spurs. Figure 4 shows the same at

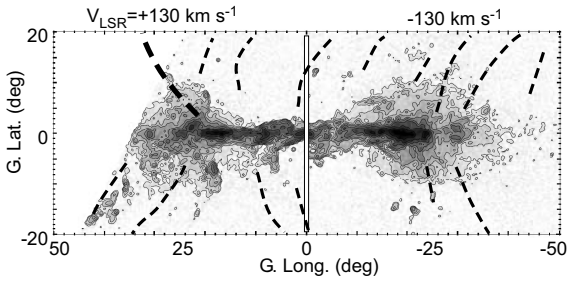

Fig. 3. HI channel map at $V_{\rm lsr} = \pm 130$ km s^{-1}. Note the absense of the HI halo inside $|l| <\sim 20^\circ$. Radio continuum spurs are indicated by dashed lines, and an HI spur emerging from the dense HI disc coincides with the NPS (thick dashed line).

$V_{\rm lsr} = 130$ km s^{-1}, where is overlaid the BGF 1420 MHz radio continuum map taken from Sofue and Reich (1979). Both the figures demonstrate the spatial coincidence of the NPS ridge with the 3-kpc HI ring and its vertical flare. Also shown in the figure is the X-ray ridge in R7 (1.4 kev) band as obtained from a ROSAT image (Snowden et al. 1997), almost coincident but slightly inside the radio NPS.

2.3 Vertical scale heights and extents

Figure 5 shows vertical (b-directional) cross sections the HI-line brightness T at different radial velocities. The b profiles show two components with narrow and wide scale heights. We fit the distribution by two layers in gravitational equilibrium in the Z direction expressed as

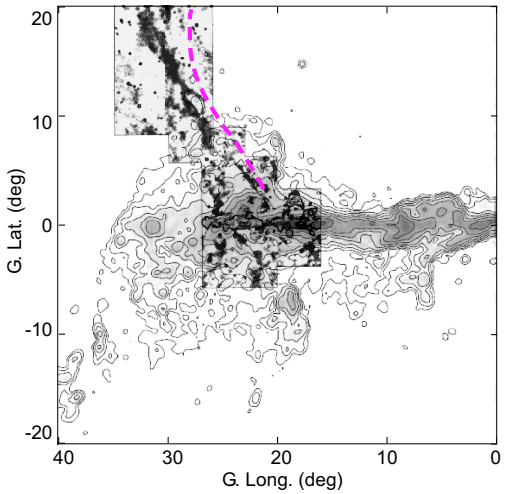

Fig. 4. Overlay of the 1.4 GHz continuum spur (Sofue and Reich 1979) on the HI channel map at $V_{\rm lsr} = +130$ km s^{-1}. The dashed line shows the X-ray R7 (1.4 keV) band ridge after correction for the extinction (Sofue 2015) made from the ROSAT image (Snowden et al. 1997).

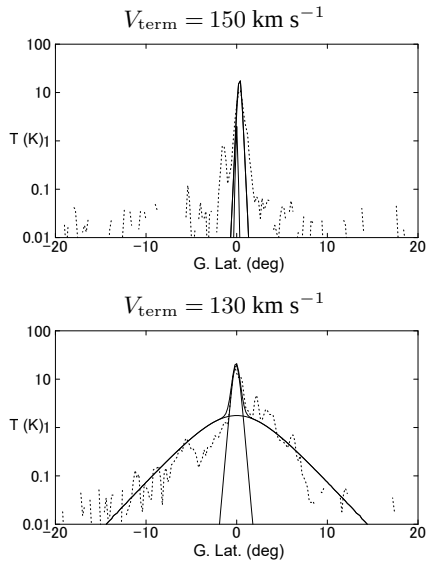

Fig. 5. Latitudinal HI intensity ($T_{\rm B}$) profile at terminal velocities $V_{\rm term} = 150$ and 130 km s^{-1}. The vertically extended feature is absent at < 130 km s^{-1}, showing the HI hole inside $l \sim 20^\circ$.

$$\rho = \rho_0 \, {\rm sech}^2(\ln(1+\sqrt{2})\, Z/h) \tag{2}$$

where h is the hydrostatic scale height of the layer (Spitzer 1942). Hereafter, we adopt $\zeta = h/\ln(1+\sqrt{2})$ as the scale height parameter, or simply the scale height, of the galactic layer. Accordingly, the brightness temperature of the HI emission at a given $V_{\rm lsr}$ is expressed by

$$T = \Sigma_i \, T_i \, {\rm sech}^2(Z/\zeta_i), \tag{3}$$

where T_i and ζ_i are the temperature at the midplane and the scale height of the i-th components, respectively. Here, $i = 1$ and 2 represent the disc and halo components, respectively.

By the χ^2 method we deconvolved the b distribution of T into two components, and determined T_i and ζ_i. The inner distribution at $V_{\rm lsr} > 150$ km s^{-1}, the b profiles are fitted by one-disc with small scale height. On the other hand at lower velocities, the b profiles are fitted by two components with narrow and wide scale heights. The midplane temperature and scale heights corresponding to the tangential direction of the 3-kpc ring are determined to be $T_1 = 22$ K and $\zeta_1 = 0^\circ.56$ (74 pc) for the disc, and $T_2 = 5.4$ K and $\zeta_2 = 3^\circ.2$ (450 pc) for the halo component. The halo component in the figures are well fitted by the sech^2 function, indicating that the gas is in gravitational equilibrium.

The disc component, having $\zeta_1 \sim 74$ pc, represents the main HI disc in the current galactic studies (e.g. Nakanishi and Sofue 2003, 2005, 2015), which has a velocity dispersion of $\sigma_1 \sim 5-10$ km s^{-1}. The halo component, showing large $\zeta_2 \sim 450$, has an order magnitude less intensity compared to the disc. In order for the halo component to be vertically extended to this height, the velocity dispersion in the HI gas must be as large as $\sigma_2 \sim 12-25$ km s^{-1}. The HI halo can be traced up to $b \pm 10^\circ$ above the detection limit of $T \sim 0.01$ K, indicating that the outskirt is extending to height of $Z \sim \pm 1.3$ kpc

2.4 Radial density profiles by tangent method

The column density of HI and H_2 gases can be related to the brightness temperature T_i by

$$N_i = X_i \int T_i dv, \tag{4}$$

and to the local volume density n_i by

$$n_i = X_i T_i \frac{dv}{dr}, \tag{5}$$

where X_i is the conversion factor for HI ($i = 1$) and CO ($i = 2$). Using the relation $r = R_0 \cos l$, $R = r \tan l = R_0 \sin l$, and $dl/dr = 1/R_0 \sin l$ at the tangent points, we obtain

$$n_i = X_i T_i \left(\frac{V_0}{R_0} - \frac{dV}{dR} \right) \cot l. \tag{6}$$

If the rotation curve is flat, it leads to a very simple equation

$$n_i \simeq X_i T_i \frac{V_0}{R_0} \cot l. \tag{7}$$

Reading T_i on the LV diagram along the terminal velocity ridge, we can determine the radial density profile converting l to R by $R = R_0 \sin l$. Adopting the usual conversion factors and the observed Galactic rotation curve, we thus calculated the HI and molecular gas densities using the LV diagrams from the survey data.

Figure 6 shows the results along the galactic plane and along altitude at $+3^\circ$. In the figure are also shown the radio continuum excess at 408 and 1420 MHz at $b = 5^\circ$, where R was calculated as above assuming the same distance. We stress that the radio NPS exactly coincides with the edge of the HI hole.

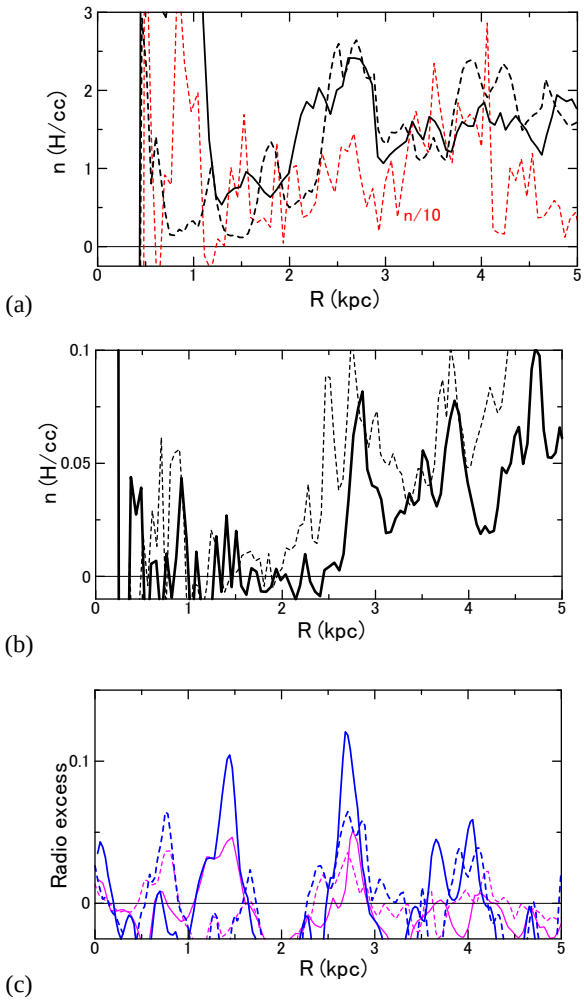

Fig. 6. (a) Volume density n of H atoms plotted against R at $b = 0^\circ$: Full=HI in Q1; dash=Q4; red dash=$0.1\times$ Molecules (CO) in Q1. (b) ibid at $b = +3^\circ$: Full=HI in Q1; dash=Q4. (c) Radio continuum excess at $b = +5^\circ$: Blue=408 MHz in Q1; dash=Q4; Magenda=1420 MHz in Q1; dash=Q4.

The HI hole is now evident in the halo at $b = 3^\circ$ (~ 400 pc) as the almost empty region inside $R = 2.8$ kpc. The HI density inside the hole is as low as $n_{\rm HI} \leq\sim 5 \times 10^{-3}$ H cm^{-3}. Beyond this radius, the intensity suddenly increases to a sharp peak at $R = 2.9$ kpc. The density in this HI wall is $n_{\rm HI} \sim 0.08$. The full radial width at half-density of the wall is measured to be $\Delta R \simeq 0.15$ kpc in the first quadrant (Q1 or $0^\circ \leq l \leq 90^\circ$). About the same structure is observed in the 4th quadrant (Q4: $270^\circ \leq l \leq 360^\circ$)

In the galactic plane ($b = 0^\circ$), the HI profile is similar, but milder. The intensity peak corresponding to the wall appears at $R = 2.7$ kpc, corresponding to the originally recognized 3-kpc expanding HI ring. The peak density of the HI gas is $n_{\rm HI} \sim 2.5$ H cm^{-3}, and the full radial width of the ring is $\Delta R \simeq 0.3$ kpc.

The molecular disc in the galactic plane is more clumpy than HI, but shows a globally flat distribution an has a small peak corresponding at $R \sim 2.6$ kpc to the 3-kpc ring with a peak density of $n_{\rm H_2} \sim 13$H cm^{-3}. Note that the molecular density scale is multiplied by 1/10 in figure 6. It is interesting to point out that the molecular fraction (molecular density/total density) is $f_{\rm mol} \simeq 0.82$, significantly lower than that at the 4-kpc molecular ring of $f_{\rm mol} \simeq 0.90$.

The parameters as determined above are summarized in table 1. Using these parameters we calculated the total mass of the ring structures, assuming a perfect ring around the GC with the constant peak densities. We also calculate the kinetic energy, assuming that the expansion velocities are all $V_{\rm expa} = 50$ km s^{-1}. The derived quantities are listed in table 1.

3 Origin of HI Hole

We now examine if the HI halo hole can be explained by sweeping of the disc and halo gas by an explosive event in the Galactic Center based on the bipolar-hyper-shell (BHS) model of the NPS (Sofue 2000; Sofue et al. 2016). The propagation of a shock wave from the Centre is calculated using the Sakashita's (1971) method to trace radial ray paths of an adiabatic shock wave.

The unperturbed gas disc and halo are assumed to be composed of a stratified layers with density distributions represented by the hydrostatic equilibrium in the Z direction (Spitzer 1942). It is assumed that the discs are further embedded in an intergalactic gas with uniform, low-density gas. We express the density distribution as

$$\rho = \Sigma \rho_i \, {\rm sech}^2(Z/\zeta_i). \tag{8}$$

Here, $i = 1$, 2, and 3 represent the disc, HI halo, and a constant background. We here take $\rho_1 = 1$, $\rho_2 = 0.1$, and $\rho_3 = 10^{-5}$ H cm^{-3}, and $\zeta_1 = 50$, $\zeta_2 = 500$ pc, and $\zeta_3 = \infty$.

Figure 7 shows the calculated result for an initial injection energy $E_0 = 1.8 \times 10^{55}$ erg. The shock front is drawn in the (R, Z) plane at every 10^6 y. The shock wave front expands almost spherically in the initial moment. As it expands, the front shape becomes elongated in the vertical direction due to the steep decrease of the density toward the halo. As the shock wave is blown off into the halo, the front shape gets dumbbell shaped, making a BHS. The dumbbell's equator is sharply pinched by the dense disc at the galactic plane. At elapsed time of $t \sim 10^7$ y, the BHS front approximately mimics the NPS, SPS, NPS-W and SPS-W.

The observed density profile near the galactic plane in figure 6 indicates that the density jump from inside to the 3-kpc ring is 3 K/ 0.7 K ~ 4, conincident with the density jump in the adiabatic shock wave as modeled here. On the other hand, the density jump is much higher in the off-plane wall at $b = 3^\circ$, exceeding ~ 10 times, much larger than that for the adiabatic shock. This may be due to the high density in the shock front

Table 1. Parameters of the 3-kpc Ring

	Disc CO ring	Disc HI ring	Halo HI wall	HI halo hole	Total
Radius, R (kpc)	2.7	2.7	2.9	2.7	—
Scale height, h (kpc)	0.07	0.07	0.4	> 1	—
Width, ΔR (kpc)	0.15	0.3	0.15	—	—
Density, n (H cm^{-3})	13	2.5	0.1	$< 5 \times 10^{-3}$	—
Mass, M ($M_\odot$)	1.1×10^8	4.3×10^7	0.6×10^7	—	1.6×10^8
Expa. velo.†, $V_{\rm expa}$ (km s^{-1})	53	53	53	—	—
Kin. Energy, $E_{\rm kin}$ (erg)	3.1×10^{54}	1.3×10^{54}	1.5×10^{53}	—	4.7×10^{54}

† Cohen and Davies (1976).

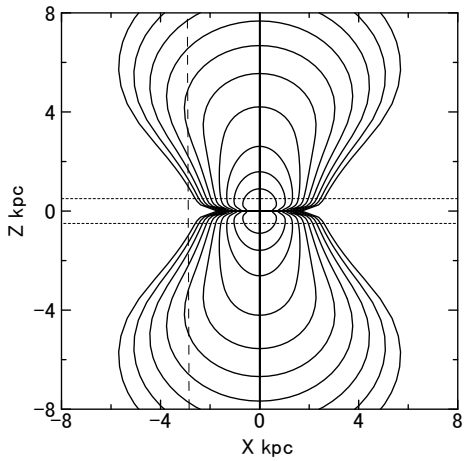

Fig. 7. Propagation of the shock front in the disc and halo. The fronts are drawn every 10^6 y.

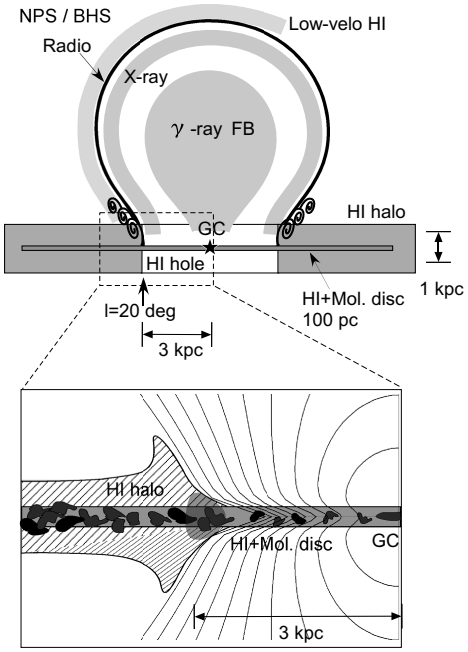

Fig. 8. Schematic relation among the NPS (BHS), 2.7-kpc expanding ring, 2.9-kpc HI hole, HI halo, and the HI+H_2 disc. Some related objects such as the X-ray NPS, Fermi Bubbles are also drawn concentric. The bottom panel enlarges the 3-kpc ring region contacting the shock front as predicted by the shock propagation solution from the Galactic Centre.

where the gas is totally ionized to X-ray temperature, leaving no HI inside the front. However, detailed spatial correlation analysis is not easy because of the tangential lines of sights through the curved shock front, along which emissions from the near- and far side structures are contaminated.

The expanding velocity of the front at intermediate latitudes $\theta \sim 10 - 20^\circ$ corresponding to the main NPS ridge is $V_{\rm expa} \sim 300$ km s^{-1}. This velocity is coincident with the required velocity to heat the shocked gas to a temperature $\sim 10^7$ K responsible to the observed X-ray emission in the NPS (Snowden et at al. 1997; Sofue et al. 2016). Note, however, the shock-heated and compressed gas inside the shock front is no more neutral (HI), but is ionized to X-ray temperatures, and is, therefore, not observed in the HI line emission. The HI wall outside the shock front is in a pre-shock compression stage, and is observed as the expanding ring, which is still slow, as observed to be expanding at $V_{\rm expa} \sim 50$ km s^{-1}, and approximately obeys the normal galactic rotation.

4 Discussion

4.1 Summary

Analyzing the HI and radio continuum data, we showed that the NPS and its counter spurs are positionally coincident with the tangential directions of the 3-kpc expanding HI ring. The HI halo inside this radius is almost empty, making a giant HI halo hole. Outside $R \sim 3$ kpc, where the disc and halo is not disturbed by the shock wave from the centre, the HI gas exhibits sech^2 density profile in the Z direction with the scale height $h_2 \sim 0.5$ kpc. Figure 8 summarizes the variuos features observed in HI, molecular lines, radio, X-ray, and γ rays.

4.2 Some difficulties in the models

The hydorodynamical BHS model (Sofue et al. 2016) well explains the NPS and its X-ray geometry and spectra, hence the shocked gas temperatures. However, the galactic plane was shown to exhibit a bow-shock front around the dense and cool disc, and the front position appeared at about a half radius of the shells. This situation is also found in the present simple calculation in figure 7. Sanders and Prendergast (1974) had to assume an energy as large as $\sim 3 \times 10^{58}$ erg in order to accelerate the 3-kpc ring, and also showed that the shock wave destroys the disc, leaving the ring as a small portion of a compressed disc gas left after a spill over of the global flow. Such a problem could be solved by considering refraction and focusing of the waves onto the ring (Sofue 1977, 1984).

If we assume that the unperturbed gas disc and halo before the GC explosion had already a much smaller density or a hole around the GC, this problem would be eased. Such a hollow halo would be possible, if the GC explosions occurr intermittently, so that the gas around the GC is always blown off, or kept at high-temperature. The high temperature plasma observed around the GC (Snowden et al. 1997; Uchiyama et al. 2013; Su et al. 2010) could be evidence for such multiple events.

These problems are not encountered in the bar hypothesis, in which no energetic explosion is required. On the other hand, the largely extended vertical structure of the HI wall and the almost empty hole in the HI halo might not be easy to be explained by the bar models

4.3 Low-velocity HI shell

It has been suggested that low-velocity HI gas at $|V_{\rm lsr}| <\sim 50$ km s^{-1}apparently surround outside the NPS, when the radio continuum map (e.g. Halsam et al. 1982) and the all-sky HI map (e.g. Kalberla et al 2005) are compared. It is not clear if they are indeed related physically to each other. In fact, the local-velocity HI map is full of bright, often much brighter, local HI shells and filaments, so that it is difficult to confirm that the apparent HI shell surrounding NPS is indeed physically related to the radio continuum structure.

If we assume that the HI outer shell is associated with the NPS, the following scenario would be possible: The swept-up gas by the BHS is compressed to form high-temperature X-ray gas, while the densest front may have cooled down to neutral gas. The accumulated gas in the BHS in the polar cap region has not enough angular momentum to maintain the original galactic rotation. The lifted gas to the top of NPS falls toward the disc, causing negative radial velocities, canceling the galactic rotation. Since we do not have yet a model to discuss the cooling of the compressed gas to the HI temperature in the NPS, the above speculative scenario remains as a subject to be considered in the future.

References

Baba J., Saitoh T. R., Wada K., 2010, PASJ, 62, 1413

Bania T. M., 1977, ApJ, 216, 381

Binney J., Gerhard O. E., Stark A. A., Bally J., Uchida K. I., 1991, MNRAS, 252, 210

Cohen R. J., Davies R. D., 1976, MNRAS, 175, 1

Crocker R. M., Bicknell G. V., Taylor A. M., Carretti E., 2015, ApJ, 808, 107

Dame, T. M., Hartman, D., Thaddeus, P. 2001, ApJ 547, 792.

Dame T. M., Thaddeus P., 2008, ApJ, 683, L143

Englmaier P., Gerhard O., 1999, MNRAS, 304, 512

Fux R., 1999, A&A, 345, 787

García P., Bronfman L., Nyman L.-

A., Dame T. M., Luna A., 2014, ApJS, 212, 2

Haslam, C. G. T., Salter, C. J., Stoffel, H., & Wilson, W. E. 1982, AAS, 47, 1

Honma M., Nagayama T., Sakai N., 2015, PASJ, 67, 70

Jonas, J. L., Baart, E. E., & Nicolson, G. D. 1998, MNRAS, 297, 977

Kalberla, P. M. W., Burton, W. B., Hartmann, D., et al. 2005, AA, 440, 775

Kalberla P. M. W., et al., 2010, A&A, 521, A17 , 722, 367

McClure-Griffiths N. M., et al., 2009, ApJS, 181, 398

Moellenhoff C., 1976, AA, 50, 105

Mulder W. A., Liem B. T., 1986, A&A, 157, 148

Nakanishi H., Sofue Y., 2016, PASJ, 68, 5

Oort J. H., 1977, ARAA, 15, 295

Reich P., Testori J. C., Reich W., 2001a, yCat, 337,

Reich P., Testori J. C., Reich W., 2001b, A&A, 376, 861

Sakashita S., 1971, ApSS, 14, 431

Sanders R. H., Prendergast K. H., 1974, ApJ, 188, 489

Snowden S. L., et al., 1997, ApJ, 485, 125

Sofue Y., 1976, PASJ, 28, 19

Sofue, Y. 1977, AA 60, 327.

Sofue Y., 1984, PASJ, 36, 539

Sofue, Y. 1994, ApJ.L., 431, L91

Sofue, Y. 2000, ApJ, 540, 224

Sofue, Y. 2017, MNRAS, submitted.

Sofue Y., Habe A., Kataoka J., Totani T., Inoue Y., Nakashima S., Matsui H., Akita M., 2016, MNRAS, 459, 108

Sofue Y., Nakanishi H., 2016, PASJ, 68, 63

Sofue, Y. and Reich, W. 1979 AAS 38, 251

Spitzer L., Jr., 1942, ApJ, 95, 329

Su, M., Slatyer, T. R., and Finkbeiner, D. P. 2010, ApJ, 724, 1044

Uchiyama H., Nobukawa M., Tsuru T. G., Koyama K., 2013, PASJ, 65, 19